Characterisation of coronary atherosclerotic morphology by spectral analysis of radiofrequency signal: in vitro intravascular ultrasound study with histological and radiological validation

M P Moore, T Spencer, D M Salter, P P Kearney, T R D Shaw, I R Starkey, P J Fitzgerald, R Erbel, A Lange, N W McDicken, G R Sutherland, K A A Fox

Abstract

***Objective*—To determine whether spectral analysis of unprocessed radiofrequency (RF) signal offers advantages over standard videodensitometric analysis in identifying the morphology of coronary atherosclerotic plaques.**

***Methods*—97 regions of interest (ROI) were imaged at 30 MHz from postmortem, pressure perfused (80 mm Hg) coronary arteries in saline baths. RF data were digitised at 250 MHz. Two different sizes of ROI were identified from scan converted images, and relative amplitudes of different frequency components were analysed from raw data. Normalised spectra was used to calculate spectral slope (dB/MHz), y-axis intercept (dB), mean power (dB), and maximum power (dB) over a given bandwidth (17–42 MHz). RF images were constructed and compared with comparative histology derived from microscopy and radiological techniques in three dimensions.**

***Results*—Mean power was similar from dense fibrotic tissue and heavy calcium, but spectral slope was steeper in heavy calcium (−0.45 (0.1)) than in dense fibrotic tissue (−0.31 (0.1)), and maximum power was higher for heavy calcium (−7.7 (2.0)) than for dense fibrotic tissue (−10.2 (3.9)). Maximum power was significantly higher in heavy calcium (−7.7 (2.0) dB) and dense fibrotic tissue (−10.2 (3.9) dB) than in microcalcification (−13.9 (3.8) dB). Y-axis intercept was higher in microcalcification (−5.8 (1.1) dB) than in moderately fibrotic tissue (−11.9 (2.0) dB). Moderate and dense fibrotic tissue were discriminated with mean power: moderate −20.2 (1.1) dB, dense −14.7 (3.7) dB; and y-axis intercept: moderate −11.9 (2.0) dB, dense −5.5 (5.4) dB. Different densities of fibrosis, loose, moderate, and dense, were discriminated with both y-axis intercept, spectral slope, and mean power. Lipid could be differentiated from other types of plaque tissue on the basis of spectral slope, lipid −0.17 (0.08). Also y-axis intercept from lipid (−17.6 (3.9)) differed significantly from moderately fibrotic tissue, dense fibrotic tissue, microcalcification, and heavy calcium. No significant differences in any of the measured parameters were seen between the results obtained from small and large ROIs.**

***Conclusion*—Frequency based spectral analysis of unprocessed ultrasound signal may lead to accurate identification of atherosclerotic plaque morphology.**

(*Heart* 1998;**79**:459–467)

Keywords: tissue characterisation; intravascular ultrasound; spectral analysis; radiofrequency data

Department of Cardiology, University of Edinburgh, Edinburgh, UK
M P Moore
P P Kearney
T R D Shaw
I R Starkey
A Lange
K A A Fox
G R Sutherland
D M Salter

Department of Medical Physics, University of Edinburgh
T Spencer
N W McDicken

Cardiovascular Research Institute, University of California, San Francisco, California, USA
P J Fitzgerald

Department of Cardiology, University of Essen, Essen, Germany
R Erbel

Correspondence to:
Dr M P Moore,
41 Crystal Terrace,,
Burlingame, CA 94010,
USA.

Accepted for publication
14 November 1997

Previous intravascular ultrasound (IVUS) studies have shown that the presence of target lesion calcium affects both the acute and long term results of coronary interventions. After percutaneous transluminal coronary angioplasty (PTCA), a chronic reduction in total vessel area is the main operative mechanism of lumen reduction and is more prevalent in lesions with mixed or calcific composition.[1] Calcified lesions are more prone to dissect than non-calcified lesions[2] and restenosis has been shown to occur in a high percentage of patients (78%) with deep medial dissections.[3] The pre-intervention lesion arc of calcium measured by IVUS has also been shown to be a strong, consistent predictor of the effectiveness and results of directional coronary atherectomy.[4] Angiography is only moderately sensitive (60%) for the detection of extensive calcification and even less sensitive for the presence of milder degrees of atherosclerosis.[5] Conventional IVUS is more sensitive in detecting calcified plaques (80%), but because of the inability of IVUS to detect microcalcification and different densities of coronary fibrosis, its role in the acute and long term outcome of interventional procedures is uncertain.

Postmortem studies indicate that in fatal myocardial infarction intraluminal thrombus is often found sitting on a fissured and dissected lipid pool with a thin fibrotic cap, implying low stability of these lipid rich lesions,[6] which may have been haemodynamically mild when stabile. Lipid rich lesions may also be present in angiographically normal coronary arteries: only 6.8% of angiographically normal reference segments are deemed normal by IVUS.[7] Some recent IVUS studies suggest that calcification is present in about 80% of the plaques associated with acute myocardial infarction and that cross sectional area stenosis in acute myocardial infarction is on average 52% and results mainly from highly echogenic material.[3]

What the ultrasonic characteristics are of plaques prone to rupture, how to identify unstable plaques, and how to treat angiographically normal yet diseased regions are important and still unanswered questions. With improved morphological characterisation of the plaque, we might be able to identify unstable plaques, plaques that respond well to lipid lowering treatment, and, in the long term, characterise the morphological changes caused by our treatment of choice.

IVUS is an established technique for demonstrating atherosclerotic plaque size in vivo but, on the basis of previous in vitro studies, the accuracy of conventional videodensitometric analysis in identifying different atherosclerotic plaque types is limited and can roughly differentiate only three basic types of plaque: highly echoreflective regions with acoustic shadows often corresponding to calcified tissue; echodense areas representing fibrosis or microcalcification; and sonolucent intimal thickening corresponding to fibrotic, thrombotic/haemorrhagic or lipid tissue, or a mixture of these elements.[8–11] More objective, quantitative texture analysis of videodensitometric data has not led to significant improvements in the ability to discriminate between basic plaque types.[12 13] Videodensitometric analysis uses grey scale values (typically 0 (black) to 255 (white)) to describe the strength of the ultrasound signal on the image display. Although videodensitometric analysis is the most straightforward technique for quantifying IVUS data, these data are at the end of a long processing chain, including many non-linear stages the purpose of which is to provide a pleasing image on the screen. The problem with using such data for further analysis is that their relation with the original acoustic signal has been highly distorted and can even be altered by display controls such as brightness and gain.

In contrast to this, if access to the raw ultrasound signal is possible, then the analysis of the radiofrequency (RF) data results in an inherently more accurate and reproducible technique for measuring tissue properties. The RF signal is usually accessed very early on in the processing change, before demodulation and scan conversion, and is directly related to the interaction of the ultrasound in the tissue wall. The analysis of RF data permits more reproducible measurement of the ultrasound signal and enables the application of more advanced signal processing techniques, such as frequency based analyses.[14] Previous studies on vessel wall[15 16] and thrombus[17] suggest that analysis of backscattered RF data may offer an objective and reproducible method of categorising plaque components.

This study aimed to assess whether a frequency based quantitative analysis of raw RF data could identify accurately different atherosclerotic plaque types classified as lipid, loose fibrotic tissue, moderately fibrotic tissue, dense fibrotic tissue, heavy calcium, and microcalcification determined by a detailed histological examination.

Methods

IN VITRO IMAGING PROTOCOL

Side branches of postmortem right or left coronary arteries were tied and the arteries were mounted in a flow phantom for imaging within half an hour after dissection from the heart. The interval between death to excision ranged from 8 to 12 hours. Physiological pressure (80 mm Hg) was provided by an inflatable pressure cuff and saline bag connected to the proximal end of the perfusion system, and was monitored with a pressure transducer connected to the distal end of the phantom. Vessels were imaged in a saline bath at room temperature (24°C) and the IVUS catheter was introduced into the vessel section via a water tight valve of the modified vessel sheath. Depending on the degree of atherosclerosis and types of plaques present, three to nine cross sections from each artery were collected with a Hewlett Packard Intravascular Scanner (Hewlett Packard Co, Andover, Massachusetts, USA) and both unprocessed RF signal and video output data were recorded. The imaged sites were marked with a silk suture for histological location, and the clockwise and longitudinal position of the suture was recorded. From each imaged cross section, four to nine regions of interest were chosen for spectral analysis of RF data using the topology of both anatomical and pathological landmarks evident on both histology and ultrasound. Location of the landmarks was then used to identify the histologically different wall compositions that had similar videodensitometric appearance.

DATA ACQUISITION

Raw ultrasound signals for this study were collected from the RF output of the Hewlett Packard Scanner using either new Boston Scientific 30 MHz, 3.5 F, mechanically rotated catheter transducers (Boston Scientific Corp, Watertown, Massachusetts, USA) or catheters that had been used previously for clinical investigations and flushed with air and hung vertically to maximise their operational lifetime for in vitro work.

Each transmitted line of raw ultrasound signal was digitised by a Tektronix RTD720A real-time digitiser (Tektronix Inc, Beaverton, Oregon, USA) with 512 kbyte of fast random access memory (RAM). A complete 360° scan of 240 lines was captured in real-time—that is, in one frame period of 33 ms for an IVUS frame rate of 30 frames/second. Each line was digitised with a sampling rate of 250 MHz (8 bits vertical resolution) and consisted of 2048 sample points, giving a scan depth of ~ 6 mm. The digitiser was controlled by an IBM compatible personal computer with a 60 MHz Pentium processor and 16 Mbytes of RAM, via an IEEE-488 general purpose interface bus. Data capture was initiated by a single keystroke: this software trigger was combined with frame and line timing pulses from the IVUS scanner to achieve frame synchronisation with the scanner's video images.[18] Captured RF data for one frame (~ 492 kbytes) was automatically transferred to the hard disk of the computer

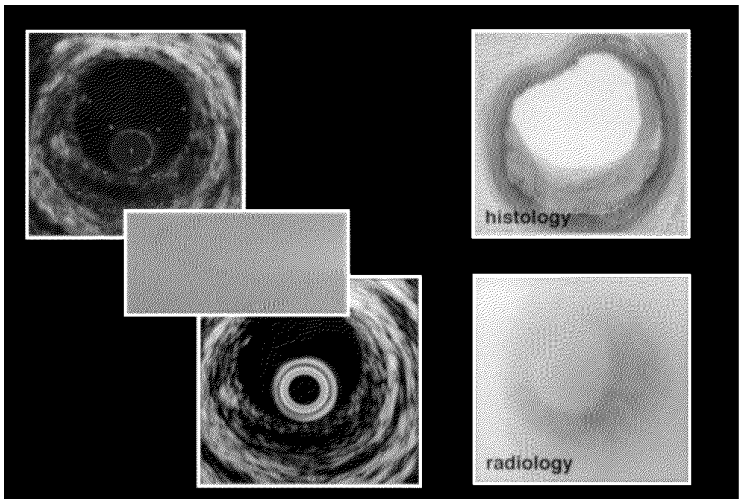

Figure 1 Scan converted RF image (upper left), raw ultrasound data (middle left), normal videoimage (lower left), histology, and radiology from corresponding vessel site (right).

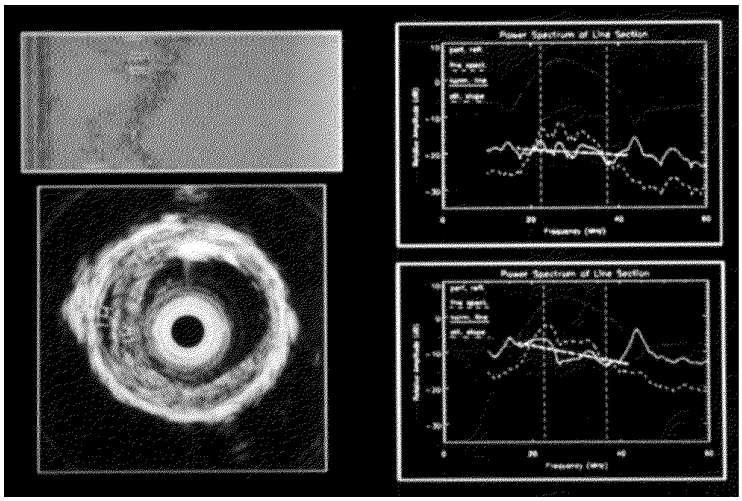

Figure 2 Spectral analysis. (Upper left) Raw, unprocessed radiofrequency data. (Lower left) Scan converted image of the area of interest. (Right) Power spectrum from two regions of interest.

(maximum transfer rate 500 kbyte/second). After collection, the data were transferred to a magneto-optical disk for archiving.

SIGNAL PROCESSING

For each raw dataset a scan converted image was constructed for orientation within the data and for comparison with histological sections. This was achieved by demodulating each line with the Hilbert transform, sub-sampling the resultant array and scan converting this to produce a circular image. A 512 × 512 pixel size of scan converted image gave an adequate display of image details and permitted the viewing of the raw data image, graphs, and text windows at the same time (fig 1). When the reflected ultrasound signal is analysed in terms of its frequency components a power spectrum results. This graph displays the relative magnitudes of all the frequencies within the returned signal (the received pulse being formed of the superposition of sinusoidal waves of different frequencies and magnitudes). The shape of this spectral graph can be analysed within a range of frequencies either side of the transducer's central frequency. This range is usually limited to frequencies that produce a sufficiently high signal, and is called the bandwidth. General trends can often be seen within this bandwidth, or the curve may be characteristic of the tissue being analysed. If a straight line is fitted to the power spectrum within the bandwidth (by liner regression) this gives an indication of the relation between backscattered ultrasonic frequency and the tissue—for example, a positive slope will indicate that relatively more ultrasonic power has been received at higher frequencies than at the lower end of the bandwidth. The extrapolation of this line to the y-axis (0 Hz) gives a value (in dB) that reflects both the frequency dependent characteristic of the tissue sample and its overall (mean) backscattering power within the bandwidth.

Tissue characterisation was based on parameters derived from power spectra calculated from defined sections of raw data. The size of the sections (regions of interest, ROI) were defined by the number of data samples along the line of site of the ultrasound beam (length) and the number of adjacent lines from which data were collected (width). To investigate the effect of the size of the ROI on the results, two different sizes of ROIs from the same area of interest were used for data collection and the corresponding results were compared to each other: 9 lines × 128 sample points = 13.5 (width) × 0.4 mm (length) (large ROI) and 5 lines × 64 sample points = 7.2 (width) × 0.2 mm (length) (small ROI). The power spectra were calculated from the Fourier-transformed line-sections and then summed over the width of the ROI, line by line. Each power magnitude in the resulting spectrum was divided by the number of lines making up the ROI, to obtain the average spectrum for that ROI (fig 2).

Power spectra were normalised with a power spectrum obtained from the signal returned by a perfect specular reflector (an optically smooth glass block). The reflector was placed 1 mm from the transducer, in water, at the angle that gave the maximum reflected amplitude of the signal. The resulting normalised spectra, which have the spectral contribution of the transducer/machine removed leaving spectra that show more clearly the frequency characteristics of the tissue, were used to extract the following frequency based parameters within a bandwidth of 17–42 MHz. (Bandwidth 17–42 MHz was selected as it corresponded to the −20 dB bandwidth of the system. Although the illustrations in this article show frequencies from 10–60 MHz, only 17–42 MHz was use to calculate the spectral parameters.[18])

- Mean power (dB)
- Maximum power (dB)
- Spectral slope (dB/MHz) (a least-squares linear regression over the given bandwidth)
- y-axis intercept of spectral slope (dB) (intercept of the straight spectral line with the y-axis at 0 Hz).

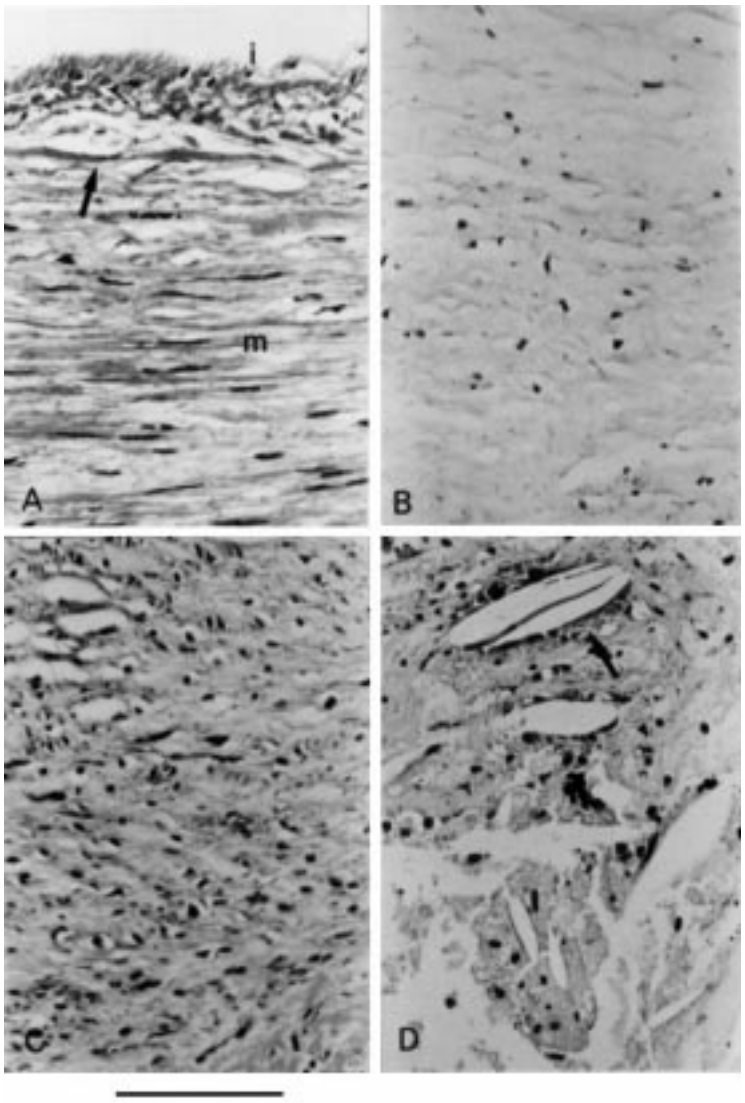

Figure 3 Morphometric features of sonolucent plaques. (A) Normal media, smooth muscle cells of the normal media (m) are separated from a thin intima (i) by an internal elastic lamina (arrow). (B) Loose fibrotic tissue, atheromatous plaque composed of loose, collagenous fibrous tissue with small numbers of cells. (C) Moderately fibrotic tissue, atheromatous plaque showing an increase in numbers of fibroblasts and smooth muscle cells, and increased amounts of stainable collagenous connective tissue. (D) Fatty tissue, atheromatous plaque with foam cells, free lipid, and cholesterol crystals (arrow).

HISTOLOGY ANALYSIS

Altogether, 97 ROIs were characterised with ultrasound and by histology. After ultrasound data collection, the vessels were pressure perfused with 4% buffered formaldehyde under 80 mm Hg of pressure for 24 hours. Routine histology stains were used to identify different components of the vessel wall (haematoxylin and eosin, Elastic-Van Gieson, Mason trichrome and alizarin red (for calcium)). Specimens were classified on the basis of histology into six subgroups (figs 3 and 4): (a) loose fibrotic tissue—loose, oedematous connective tissue with few cells and small amounts of collagen (haematoxylin and eosin); (b) moderately fibrotic tissue—increased cellularity and collagen content in comparison to (a) (haematoxylin and eosin); (c) fatty tissue—including subgroups of homogeneous areas of foam cells and lipid pools, and combinations of loose or moderate fibrosis with lipid; (d) dense fibrotic tissue—plaques consisting of dense, hyaline collagen with small numbers of cells (haematoxylin and eosin); (e) microcalcification—areas of microcalcification with plaques that could only be visualised following staining for calcium with alizarin red; and (f) calcified plaques—areas of heavy calcification that could be identified in standard haematoxylin and eosin stained sections.

After histological analysis, corresponding areas were identified from the scan converted images and spectral analysis was applied to the raw data with two different sizes of ROIs.

MORPHOLOGICAL CORRESPONDENCE

For four vessels, detailed histology, motorised pullback of IVUS catheter, and radiographs were used to test the accuracy of the location of the silk suture to identify both longitudinal and clockwise position corresponding to histology and ultrasound data. For those vessels, 10 consecutive histology slices were taken every 100 μm starting from the point of suture mark, automatic pullback software was used to capture RF data every 200 μm over the length of the vessel starting from the same suture mark, and the amount and location of calcium was identified with cross sectional and longitudinal *x* ray images (figs 5 and 6). This approach gave a fully confident correspondence of the sites of interest and the location of the suture estimated by two investigators in all cases. The histological correspondence in the rest of the studied vessels was thereafter confirmed by the location of calcium in the radiographs and with the suture mark.

STATISTICAL ANALYSIS

All results are expressed as means (SD). Intergroup comparisons were conducted with analysis of variance and the significance of difference between different plaque types was tested with non-paired Student's *t* test (Bonferroni modification). The differences between the results obtained from the two sizes of ROI were tested with paired Student's *t* test. All differences were considered significant when $p < 0.01$.

Results

IDENTIFICATION OF FATTY TISSUE

Spectral slope was the best single parameter to discriminate lipid containing tissue from fibrotic tissue. It was significantly different from each subgroup ($p < 0.01$) and there was no overlap between the standard deviations (table 1). Y-axis intercept of the power spectrum was similar in lipid and loose fibrotic tissue, but significantly higher in moderate fibrosis, dense fibrosis, and heavy calcium. Maximum and mean powers recorded from the lipid containing tissue did not differ from that recorded from the loose fibrotic tissue, but mean power was significantly less from lipid than from moderate and dense fibrosis and from heavy calcium and microcalcification ($p < 0.01$) (table 2).

IDENTIFICATION OF CALCIFICATION

Maximum power from microcalcification was significantly higher than that measured from loose fibrotic tissue and lipid, and significantly lower than maximum power from heavily calcified plaques (tables 1 and 2). Mean power from microcalcification was lower than mean power recorded from both heavy calcium and dense fibrotic tissue, and less than that recorded from loose fibrotic tissue and lipid. Moderate fibrosis and microcalcification were discriminated from each other only on the basis of y-axis intercept of the power spectrum ($p < 0.01$) (table 2).

Heavily calcified plaques had the steepest spectral slope of the power spectrum. The difference was significant when compared to every other histological subgroup except microcalcification ($p < 0.01$). Y-axis intercept was, however, higher in heavy calcium than in microcalcification and higher compared to moderate fibrosis, loose fibrotic tissue, and lipid (table 1). Maximum power and mean power from heavy calcium were also significantly higher than corresponding values measured from loose and moderately fibrotic tissue (table 2), but compared to dense fibrotic tissue, maximum, but not mean power, was able to identified heavy calcium.

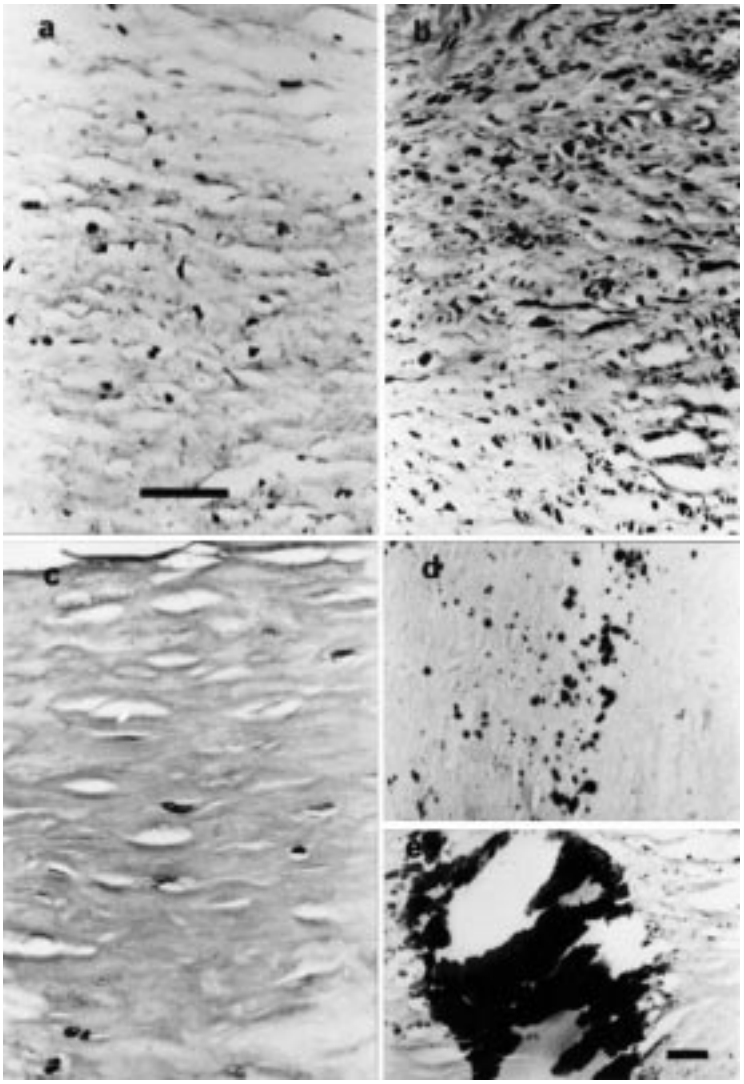

Figure 4 Morphological features of fibrotic and calcified plaques. (a) Loose fibrotic tissue. (b) Moderately fibrotic tissue. (c) Dense fibrotic tissue. (d) Microcalcification, areas of microcalcification with plaques visualised following staining for calcium with alizarin red. (e) Calcified plaques, heavy calcification identified with haematoxylin and eosin. (a–d) Original magnification ×50, bar = 100 μm; (e) original magnification ×12.5, bar = 200 μm.

Table 1 Power spectrum related parameters in coronary atherosclerotic plaques

Group	*n*	*Gradient (dB/MHz)*	*Y-axis intercept (dB)*
Lipid	42	−0.17 (0.08)	−17.6 (3.9)
LFT	23	−0.06 (0.10)	−20.9 (3.8)
MFT	12	−0.28 (0.05)	−11.9 (2.0)
DFT	10	−0.31 (0.12)	−5.5 (5.4)
mCa	5	−0.36 (0.09)	−5.8 (1.1)
Calcium	8	−0.45 (0.10)	−0.73 (3.01)

LFT, loose fibrotic tissue, MFT, moderately fibrotic tissue, DFT, dense fibrotic tissue, mCa, microcalcification.

FIBROTIC INTIMAL THICKENING

All different fibrotic tissue subtypes—loose, moderate, and dense fibrotic tissue—were discriminated from each other by the combination of different parameters derived from the spectral slope analysis. The power related parameters presented in table 1 show clearly that as the amount of extracellular collagen increases, the amount of reflected ultrasound energy increases significantly ($p < 0.001$ between each group).

The y-axis intercept and the slope of the power spectrum were also significantly different between different densities of fibrotic tissue (fig 7). Y-axis intercept was highest in the dense fibrotic tissue and lowest in the loose fibrotic tissue ($p < 0.01$), and the slope of the power spectrum increased significantly with each subgroup being negative and steepest in the dense fibrotic tissue and almost zero in the loose fibrotic tissue.

SMALL *v* LARGE REGIONS OF INTEREST

To examine whether the size of the ROI had any impact on the results, two different sizes of ROI from the same plaque type were com-

Table 2 Power related parameters in coronary atherosclerotic plaques

Group	*n*	*Mean power (dB)*	*Max power (dB)*
Lipid	42	−22.5 (1.9)	−18.6 (2.3)
LFT	23	−22.9 (1.9)	−19.1 (1.4)
MFT	12	−20.2 (1.1)	−15.7 (1.5)
DFT	10	−14.7 (3.7)	−10.2 (3.9)
mCa	5	−18.8 (3.2)	−13.9 (3.8)
Calcium	8	−14.0 (2.4)	−7.7 (2.0)

LFT, loose fibrotic tissue; MFT, moderately fibrotic tissue; DFT, dense fibrotic tissue; mCa, microcalcification.

Table 3 Measured spectral analysis parameters in two different size of regions of interest (ROI)

	Small ROI	*Large ROI*
Power (dB)		
Maximum	−16.6 (4.5)	−17.3 (4.7)
Minimum	−26.2 (4.4)	−27.3 (5.3)
Mean	−21.2 (4.4)	−22.3 (4.7)
At 40 MHz	−21.5 (4.7)	−22.7 (3.2)
Frequency at max power	25.9 (9.2)	24.9 (10.6)
Frequency at min power	33.7 (5.5)	32.6 (5.0)
Spectral slope	−0.16 (0.17)	−0.16 (0.17)
Y-axis intercept (dB)	−16.5 (8.7)	−17.4 (8.9)

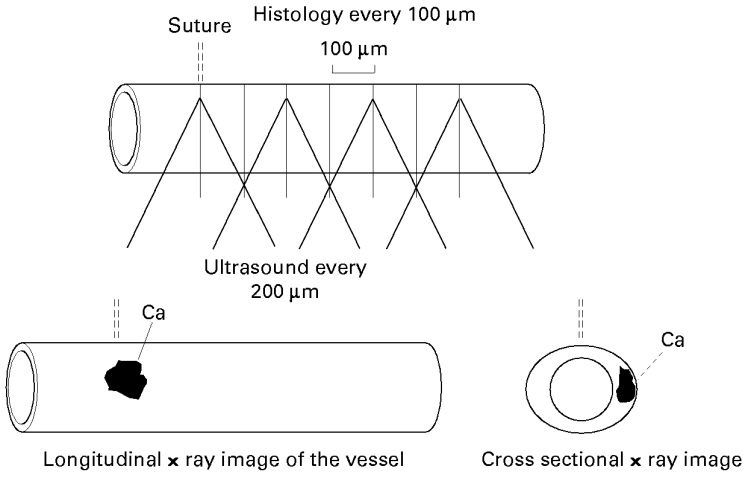

Figure 5 The validation of histological correspondence was achieved by comparing ultrasound images with the comparative histology derived from microscopy (histology slices were taken every 100 µm from the suture mark corresponding to the beginning of the motorised pullback of the IVUS catheter set to record data every 200 µm) and radiology techniques (radiograph of the vessel before histology to localise the clockwise and horizontal position of heavy calcium).

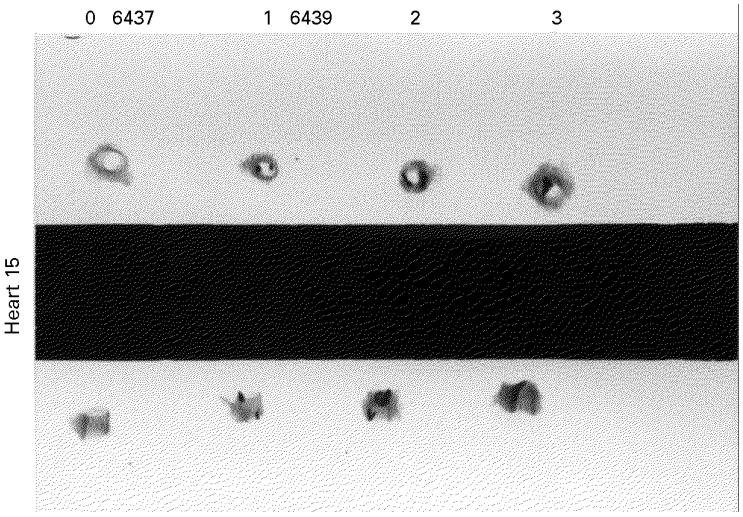

Figure 6 Identification and localisation of calcium with longitudinal and cross sectional radiographs of coronary arteries from heart 15: left anterior descending (6437; 0) and three sites from the right coronary artery (6439; 1, 2, 3).

pared. When all parameters were analysed on the basis of the size of the region, no significant differences were found between the two groups (table 3).

Discussion

The results of the present study demonstrate that an increase in the amount of extracellular collagen in the fibrotic intimal thickening leads to an increase in the amount of reflected ultrasound energy. This is in accordance with previous studies demonstrating high echoreflectivity of fibrotic tissue.[19] However, additional parameters were needed to discriminate other plaque types from each other, especially to identify lipid from loose and moderately fibrotic tissue, and to identify dense fibrosis from calcium and microcalcification.

Atherosclerotic plaque is composed of varying degrees of lipid, smooth muscle cells, fibrous and elastic tissue, and calcium. Collections of lipid are weakly echoreflective and can be seen as anechoic regions within the vessel wall. Unfortunately, similar hypoechoic areas can also arise from loose fibrotic tissue, thrombus, local shadowing by neighbouring or overlying calcium, or can be due to limitations in the dynamic range of the instrument. When using grey scale criteria, the sensitivity of identifying lipid has been reported to be only about 46%.[12] The results of the present study demonstrate that loose fibrotic tissue and lipid containing tissue reflect almost the same amount of ultrasound energy and explain why current videoimage interpretation has difficulties discriminating those atherosclerotic plaques from each other. Spectral analysis of unprocessed ultrasound data has, however, significant potential to discriminate these sonolucent plaques from each other as lipid and loose fibrotic tissue seem to have different spectral characteristics. Lipid containing tissue reflects more ultrasound energy when imaged with lower frequencies than when imaged with high frequencies resulting in a more steep spectral slope, while loose fibrotic tissue reflects almost the same amount of energy with all imaged frequencies.

In dystrophic calcification, the amount of plasma calcium is normal and tissue calcification occurs secondary to local changes in the affected tissue where calcification is normally not present. It is predominantly found (a) in areas of abnormal extracellular protein synthesis, such as the changes seen in the walls of arteries in aging, hypertension, and diabetes; (b) in tissue death, such as the necrotic lipid debris of atheromatous plaque, fat necrosis, and old infarcts; and (c) in old blood clots in veins.[20] Heavily calcified plaques are more echoreflective than any of the other plaque types and, from the conventional videoimages, the brightness and reverberations behind the calcified plaque have been the two most reliable features for identifying calcific lesions.[21] Interestingly, on the basis of the present results, dense fibrosis reflects on average as much ultrasound energy as calcified plaques do. Only the maximum power and the steepness of the spectral slope were significantly higher for heavy calcium than for dense fibrotic tissue. This difference in the uniformity of the reflected energy between dense fibrotic tissue and heavy calcium might be caused by a variation in the spatial features of these different atherosclerotic components of the vessel wall as seen in fig 4. The brightness of the echosignal alone is therefore not sufficient to identify heavy calcium from dense fibrosis when interpreting current videoimages. The reverberations behind calcified plaques, related to the high maximum power of the reflected ultrasound energy, are thus important evidence of the presence of calcium.

According to the present results, microcalcification reflects less energy than heavily calcified plaques and the slope of the power spectrum is significantly less for microcalcification than for heavy calcium. Histologically the first signs of mineral deposition are either intracellular (often in mitochondria) or extracellular (in matrix vesicles) leading to the

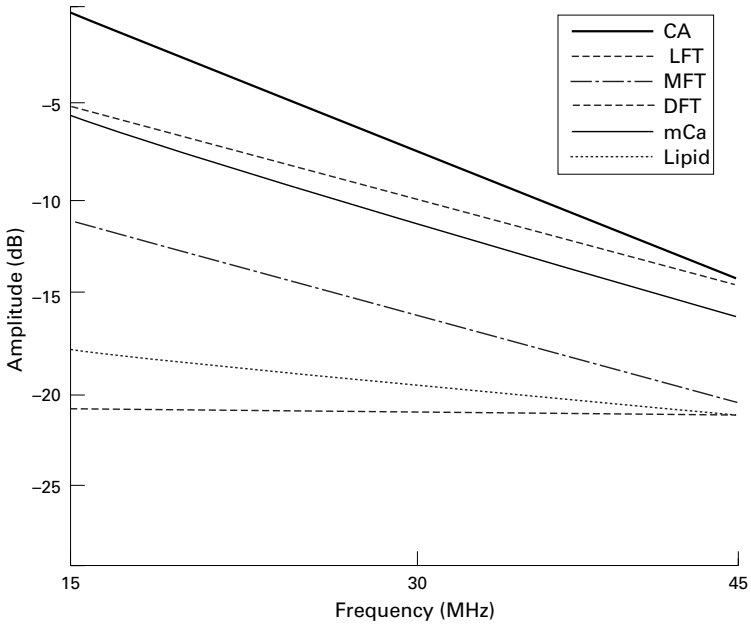

Figure 7 Power spectrum of lipid, loose (LFT), moderate (MFT), and dense fibrosis (DFT), heavy calcium (CA), and microcalcification (mCa).

propagation phase of crystal lattice formation.[20] At the beginning of mineral deposition, the size of the reflecting unit is small compared with heavily calcified plaques and therefore, with high frequencies, the behaviour of reflected ultrasound energy may be more scattering than specular in nature. When propagating ultrasound interacts with tissue whose structure can be considered, acoustically, to be composed of a random distribution of scatters of a size many times smaller that the wavelength of the sound, then omni-directional scattering takes place. The component of this so-called Raleigh scattering, which is detected by the transceiver is, by definition, that which has been scattered at 180° with respect to the incident beam. This is known a backscatter. Scattering of the propagating ultrasound decreases the amount of reflected ultrasound energy and changes the frequency dependent properties of the imaged structure altering the slope of the power spectrum[22] as seen in the present study. The present study demonstrates further that, although microcalcification reflects slightly more ultrasound energy than moderate fibrosis and less than dense fibrosis, the echoreflectivity of the plaque—the brightness of the videoimage—cannot be used alone to identify moderate fibrosis from microcalcification as the difference in the brightness of the videoimage between these two plaque types is extremely subtle.

Attenuation includes losses of ultrasound energy due to reflection, refraction, absorption, and scattering. Collagen has been shown to be an important factor responsible for attenuation in soft tissues and the increase of attenuation with frequency can be approximated by a linear function of frequency.[23–25] Ultrasonic absorption coefficient has also been shown to have the same frequency dependence as attenuation coefficient.[26] Absorption increases as a function of collagen concentration and absorption per unit concentration associated with the presence of collagen is approximately four times that for the globular proteins.[23] Therefore, even relatively small changes in collagen content can have measurable effects on ultrasonic properties. This was evident in the present study, which showed that the amount of reflected ultrasound energy increased as a function of the collagen density in fibrotic tissues and can be used to help the interpretation of current videoimages when evaluating the density of the fibrotic plaque.

The slope of the power spectrum was negative in all histological subgroups; near zero from loose fibrotic tissue only, becoming more negative as the amount of extracellular collagen increased, and was steepest from calcified plaques. Although positive spectral slopes have been reported from data analysed from arterial walls,[27] negative spectral slopes computed without attenuation correction, as in the present study, have been reported from diseased arterial walls,[28] liver tissue, and ocular tumours.[29 30] The negative spectral slopes in the present study may also be explained by a higher attenuation of ultrasound energy with high frequencies from structures larger than the wavelength. This has been predicted theoretically and demonstrated empirically to produce negative spectral slopes.[22]

Both attenuation and the backscattered energy of the transmitted ultrasound are affected by the depth of the sample volume. In the present study, no correction for the frequency dependent attenuation of the intervening medium between the transducer and the region of interest was applied. Consequently, the power of the backscattered energy is likely to have a finite error associated with it. Because of the short distances of insonation and the small sizes of regions of interest, the calculation of attenuation coefficient (dB/MHz/cm) was regarded as too problematic. Therefore, in the present study, the frequency dependent attenuation caused by the intervening tissues was assumed to have a negligible affect on the calculated spectral slope parameters and the measured differences in the acoustic properties observed between different plaques were assumed to be greater than the gradual decrease of the slopes over distance.

Double blind studies on the predictive accuracy of these frequency based parameters and in vivo studies will eventually show whether spectral analysis of unprocessed data is robust enough to survive the inherent sources of error related to in vivo intravascular imaging. These include the angle dependency of the recorded ultrasound signal (in the present study the data were always acquired at orthogonal angle), the effect of cardiac cycle, blood speckle, and the normalisation of the data to exclude the frequency dependent properties of the imaging device. In addition, the distance of the transducer from the region of interest and thus the diameter of the vessel can potentially lead to the diffraction of the ultrasound signal. Diffraction correction, however, has not been shown to make any difference in the spectral slope measurements.[28]

The amplitude of the echo reflected from an interface depends on the angle at which the beam strikes the interface, the reflective properties of the tissue components, their pattern of organisation, and the dynamic range and resolution of the recording device.[31] Coronary disease will generally increase tissue density with surface irregularity diminishing, but not negating, these effects. With IVUS, the strongest signals are obtained when the catheter is central and coaxial within the vessel. Maximal reflectance occurs when the beam strikes the target at a 90° angle and decreases rapidly as the angle of intersection becomes more obtuse.[32] In the present study the angle of incidence was not standardised, which is similar to the clinical situation, but did not include the effects of vessel tortuosity. Unlike the situation in large peripheral arteries, in small diameter coronary arteries serious off axis positions are uncommon with currently used ultrasound catheters.

In vitro, mean pixel grey levels from vessel wall during blood perfusion has been shown to be about 85% of that obtained during saline perfusion.[12] In thrombus and in blood at constant haematocrit, the backscattered intensity is linearly proportional to the number of red blood cells per aggregate.[33 34] In vitro studies on the frequency dependent characteristics of flowing blood, imaged with 30 MHz central frequency have shown that the average backscatter coefficient from whole blood is near 1 dB/MHz/cm under static conditions and with high flow (1000 s^{-1}) increases to approximately 3.1 dB/MHz/cm, while the power of the integrated backscatter decreases by 13 dB.[35] These results highlight the importance of standardising the timing of IVUS imaging within the cardiac cycle when acquiring data in clinical practice because of the pulsatile nature of blood flow in coronary arteries. Recent studies on blood clots have also demonstrated that spectral and texture analysis of unprocessed IVUS signal can discriminate red from white clot and plasma.[31 32] Further work is needed to assess whether texture or spectral analysis of ultrasound data has more potential to identify thrombus and stagnant blood from other sonolucent plaque morphology.

In the current study an optically smooth glass block was used as a perfect specular reflector to normalise the power spectrum. Further technical work is needed to establish the instrument and transducer dependent variation of the spectral slope analysis in vivo. Additional technical development may include the incorporation of a perfect reflector into the imaging system itself or, perhaps, the use of other reflectors like stent struts to normalise the data.

A future role of IVUS tissue characterisation may be as a tool to facilitate decision making with regards to treatment strategy, when choosing fibrinolytic treatment *v* mechanical recanalisation, when selecting and optimising different interventional device types and sizes, and when considering secondary prophylactics (such as, lipid lowering treatment) to treat coronary atherosclerosis. Plaque characterisation might also identify plaques prone to rupture and vessel occlusion. Serial examinations of atherosclerotic lesions would provide additional insight into the pathogenetic mechanisms of coronary disease and would allow the long term follow up of changes induced by lipid lowering drugs. The results of the present study explain many of the current videoimage features of an atherosclerotic plaque, demonstrate the limitations of the videoimage interpretation of plaque morphology, and can be used as a guide when assessing plaque morphology in clinical practice. Our results suggest also that quantitative techniques based on frequency analysis of backscattered echoes, together with power calculations of the backscattered signal, may be used to improve the accuracy of IVUS in characterising coronary disease by detecting the acoustic properties of different constituents of atherosclerotic plaque.

The authors thank Dr Margaret McIntyre for providing excellent coronary arteries for this study. This study was supported by the Northern and Yorkshire Regional Health Authority (NHS Executive R&D project: IC8), Paavo Nurmi Foundation, and Finnish Cardiac Society, Finland.

1 Di Mario C, Gil R, Camenzind E, *et al*. Quantitative assessment with intracoronary ultrasound of the mechanism of restenosis after percutaneous transluminal coronary angioplasty and directional coronary atherectomy. *Am J Cardiol* 1995;**15**:772–7.
2 Fitzgerald PJ, Ports TA, Yock PG. Contribution of localized calcium deposits to dissection after angioplasty. *Circulation* 1992;**86**:64–70.
3 Jain SP, Jain A, Collins TJ, *et al*. Predictors of restenosis: a morphometric and quantitative evaluation by intravascular ultrasound. *Am Heart J* 1994;**128**:664–73.
4 Matar FA, Mintz GS, Pinnow E, *et al*. Multivariate predictors of intravascular ultrasound end points after directional coronary atherectomy. *J Am Coll Cardiol* 1995;**25**:318–24.
5 Mintz GS, Popma JJ, Pichard AD, *et al*. Patterns of calcification in coronary artery disease. A statistical analysis of intravascular ultrasound and coronary angiography. *Circulation* 1995;**91**:1959–65.
6 Davies MJ, Thomas AC. Plaque fissuring—the cause of acute myocardial infarction, sudden ischemic death, and crescendo angina. *Br Heart J* 1985;**53**:363–73.
7 Mintz GS, Painter JA, Pichard AD, *et al*. Atherosclerosis in angiographically "normal" coronary artery reference segments: an intravascular ultrasound study with clinical correlations. *J Am Coll Cardiol* 1995a;**25**:1479–85.
8 Tobis JM, Mallery J, Mahon D, *et al*. Intravascular ultrasound imaging of human coronary arteries in vivo. Analysis of tissue characterizations with comparison to in vitro histological specimens. *Circulation* 1991;**83**:913–26.
9 Nishimira RA, Edwards WD, Warnes CA, *et al*. Intravascular ultrasound imaging: in vitro validation and pathologic correlation. *J Am Coll Cardiol* 1990;**16**:145–54.
10 Gussenhoven WJ, Essed CE, Lancee CT, *et al*. Arterial wall characteristics determined by intravascular ultrasound imaging: an in vitro study. *J Am Coll Cardiol* 1989;**14**:947–52.
11 Di Mario C, The SHK, Madretsma S, *et al*. Detection and characterization of vascular lesions by intravascular ultrasound: an in vitro study corrrelated with histology. *J Am Soc Echocardiogr* 1992;**5**:135–46.
12 Peters RJG, Kok WEM, Bot H, *et al*. Characterisation of plaque components with intracoronary ultrasound imaging: an in vitro quantitative study with videodensitometry. *J Am Soc Echocardiogr* 1994;**7**:616–23.
13 Rasheed Q, Dhawale PJ, Anderson J, *et al*. Intracoronary ultrasound-defined plaque composition: computer-aided plaque characterisation and correlation with histologic samples obtained during directional coronary atherectomy. *Am Heart J* 1995;**129**:631–7.
14 Linker DT, Yock PG, Gronningsaether C, *et al*. Analysis of backscattered ultrasound from normal and diseased arterial wall. *Int J Card Imaging* 1989;**4**:177–85.
15 Landini L, Sarnelli R, Picano E, *et al*. Evaluation of frequency dependence of backscatter coefficient in normal and atherosclerotic aortic walls. *Ultrasound Med Biol* 1986; **12**:397–401.
16 Barzilai B, Saffitz JE, Miller JG, *et al*. Quantitative ultrasonic characterisation of the nature of atherosclerotic plaques in human aorta. *Circ Res 1987*;**60**:459–63.
17 Fitzgerald PJ, Connolly AJ, Watkins RD, *et al*. Distinction between soft plaque and thrombus by intravascular ultrasound tissue characterisation [abstract]. *J Am Coll Cardiol* 1991;**17**:111A.
18 Spencer T, Ramo MP, Salter DM, *et al*. Characterization of atherosclerotic plaque by spectral analysis of intravascular ultrasound: an in vitro methodology. *Ultrasound Med Biol* 1997;**23**:191–203.

19 Linker DT, Yock PG, Gronningsaether C, *et al*. Analysis of backscattered ultrasound from normal and diseased arterial wall. *Int J Card Imaging* 1989;**4**:177–85.
20 Freemont AJ. Histology of mineralised tissue. In: Hukins DWL, ed. *Calcified tissue*. Southampton: Camelot Press Ltd, 1989:21–33.
21 Gussenhoven WJ, Essed CE, Lancee CT, *et al*. Arterial wall characteristics determined by intravascular ultrasound imaging: an in vitro study. *J Am Coll Cardiol* 1989;**14**:947–52.
22 Lizzi FL, Feleppa EJ, Coleman DJ. Ultrasonic tissue characterization. In: Greenleaf JF, ed. *Tissue characterization with ultrasound*, Vol II. *Results and applications*. Florida: CRC Press, 1986:42–60.
23 Goss SA, Frizzell LA, Dunn F. Dependence of the ultrasonic properties of biological tissue on constituent proteins. *J Acoust Soc Am* 1980;**67**:1041–4.
24 Kadaba MP, Bhagat PK. Attenuation and backscattering of ultrasound in freshly excised animal tissues. *IEEE Trans Biomed Eng* 1980;**27**:76–83.
25 Goss SA, Dunn F. Ultrasonic propagation properties of collagen. *Phys Med Biol* 1980;**25**:827–37.
26 Goss SA, Frizzell LA, Dunn F. Ultrasonic absorption and attenuation in mammalian tissues. *J Acoust Soc Am* 1978;**64**:423–57.
27 Lockwood GR, Ryan LK, Hunt JW, *et al*. Measurement of the ultrasonic properties of vascular tissues and blood from 35–65 MHz. *Ultrasound Med Biol* 1991;**17**:653–66.
28 Wilson LS, Neale ML, Talhami HE, *et al*. Preliminary results from attenuation-slope mapping of plaque using intravascular ultrasound. *Ultrasound Med Biol* 1994;**20**:529–42.
29 Lizzi FL, Ostromogilsky M, Feleppa EJ, *et al*. Relationship of ultrasound parameters to features of tissue microstructure. *IEEE Transactions of Ultrasonography Ferroelectronics and Frequency Control* 1986;**33**:319–29.
30 Coleman DJ, Lizzi FL. Computerized ultrasonic tissue characterization of ocular tumors. *Am J Ophthalmol* 1983;**96**:165–75.
31 Ramo MP, Spencer T, Sutherland GR, *et al*. The in vitro characterization of red and white thrombus by spectral analysis of intravascular data: the influence of thrombus composition and age. *European Journal of Ultrasound*. [In press.]
32 Ramo MP, Spencer T, Kearney PP, *et al*. Characterization of red and white thrombus by intravascular ultrasound using radiofrequency and videodensitometric data-based texture analysis. *Ultrasound Med Biol*. [In press.]
33 Hibberd MG, Vuille C, Weyman E. Intravascular ultrasound: basic principles and role in assessing arterial morphology and function. *Am J Card Imaging* 1992;**6**:308–24.
34 De Kroon MGM, van der Wal LF, Gussenhoven WJ, *et al*. Angle-dependent backscatter from the arterial wall. *Ultrasound Med Biol* 1991;**17**:121–6.
35 Hanss van der M, Boynard M. Ultrasound backscattering from blood:hematocrit and erythrocyte aggregation dependence In: Linzer M, ed. *Ultasound tissue characterization II*. Washington, DC: National Bureau of Standards, 1979:165–9.
36 Frimerman A, Miller HI, Hallman M, *et al*. Intravasular ultrasound characterization of thrombi of different composition. *Am J Cardiol* 1994;**73**:1053–7.
37 Heiden van der M, Kroon de MG, Bom N, *et al*. Ultrasound backscatter at 30 MHz from human blood: influence of rouleau size affected by blood modification and shear rate. *Ultrasound Med Biol* 1995;**21**:817–26.